7-2010

Measurements of nonlinear harmonic waves at cracked interfaces

Hyunjo Jeong
Wonkwang University

Daniel J. Barnard
Iowa State University, dbarnard@iastate.edu

Measurements of nonlinear harmonic waves at cracked interfaces

Abstract
Nonlinear harmonic waves generated at cracked interfaces are investigated both experimentally and theoretically. A compact tension specimen is fabricated and the amplitude of transmitted wave is analyzed as a function of position along the fatigued crack surface. In order to measure as many nonlinear harmonic components as possible a broadband Lithium Niobate ($LiNbO_3$) transducers are employed together with a calibration technique for making absolute amplitude measurements with fluid-coupled receiving transducers. Cracked interfaces are shown to generate high acoustic nonlinearities which are manifested as harmonics in the power spectrum of the received signal. The first subharmonic ($f/2$) and the second harmonic ($2f$) waves are found to be dominant nonlinear components for an incident toneburst signal of frequency f. To explain the observed nonlinear behavior a partially closed crack is modeled by planar half interfaces that can account for crack parameters such as crack opening displacement and crack surface conditions. The simulation results show reasonable agreements with the experimental results.

Keywords
harmonic generation, fatigue cracks, transducers, simulation, nondestructive evaluation, QNDE

Disciplines
Materials Science and Engineering | Structures and Materials

This article appeared in *AIP Conference Proceedings* 1335 (2011): 306–313 and may be found at http://dx.doi.org/10.1063/1.3591869.

MEASUREMENTS OF NONLINEAR HARMONIC WAVES AT CRACKED INTERFACES

Hyunjo Jeong and Dan Barnard

Citation: AIP Conf. Proc. **1335**, 306 (2011); doi: 10.1063/1.3591869
View online: http://dx.doi.org/10.1063/1.3591869
View Table of Contents: http://proceedings.aip.org/dbt/dbt.jsp?KEY=APCPCS&Volume=1335&Issue=1
Published by the American Institute of Physics.

MEASUREMENTS OF NONLINEAR HARMONIC WAVES AT CRACKED INTERFACES

Hyunjo Jeong[1] and Dan Barnard[2]

[1]Division of Mechanical and Automotive Engineering, Wonkwang University, Iksan, Jeonbuk 570-749, Korea
[2]Center for Nondestructive Evaluation, Iowa State University, Ames, Iowa 50011

ABSTRACT. Nonlinear harmonic waves generated at cracked interfaces are investigated both experimentally and theoretically. A compact tension specimen is fabricated and the amplitude of transmitted wave is analyzed as a function of position along the fatigued crack surface. In order to measure as many nonlinear harmonic components as possible a broadband Lithium Niobate ($LiNbO_3$) transducers are employed together with a calibration technique for making absolute amplitude measurements with fluid-coupled receiving transducers. Cracked interfaces are shown to generate high acoustic nonlinearities which are manifested as harmonics in the power spectrum of the received signal. The first subharmonic (f/2) and the second harmonic (2f) waves are found to be dominant nonlinear components for an incident toneburst signal of frequency f. To explain the observed nonlinear behavior a partially closed crack is modeled by planar half interfaces that can account for crack parameters such as crack opening displacement and crack surface conditions. The simulation results show reasonable agreements with the experimental results.

Keywords: Acoustic Nonlinearity, Cracked Interfaces, Higher Harmonics, Subharmonics
PACS: 43.25.Dc, 43.25.Zx, 43.25.Ba

INTRODUCTION

One of the major roles of ultrasonic nondestructive inspection (NDI) is to detect and characterize crack-like flaws in critical components and structures. Both linear and nonlinear ultrasonic techniques can be applied for these purposes. When cracks are open, linear methods based on the time-of-flight-diffraction (TOFD) or a pulse-echo reflection can be a useful tool. However, when cracks are closed or partially closed, it will be more challenging to detect them because the diffracted or reflected signal is too weak. An alternative technique to overcome this limitation is nonlinear ultrasonics. Ultrasonic nonlinearity is manifested as harmonics (sub or higher) in the power spectrum of the received signal when intense ultrasonic wave is incident into imperfect interfaces. This effect is known as contact acoustic nonlinearity (CAN), and it has been the topic of many research works concerning the characterization of closed cracks or imperfect bond interfaces [1]. Earlier theoretical investigations [2-4] predicted that a weak or incompletely bonded interface will generate high second harmonics when subjected to sufficiently intense acoustic energy, and previous experiments have indicated that acoustic

Review of Progress in Quantitative Nondestructive Evaluation, Volume 30
AIP Conf. Proc. 1335, 306-313 (2011); doi: 10.1063/1.3591869

harmonic generation occur on various types of interfaces such as unbounded interfaces [5], microstructural changes [6-11], and adhesive joints [12,13].

Subharmonics are known to be generated only at the crack interface. Subharmonics is a nonlinear wave distortion where the amplitude of adjacent carriers becomes different, resulting in the period doubling and frequency of *f*/2 [14-16]. Because the higher harmonics are also generated by the piezoelectric transducers and by the electronic equipment, extraction of subharmonic response could be more reliable indicators of the crack damage. Yamanaka et al. [17] investigated the detailed feature of subharmonics generated at the closed cracks and applied the concept of subharmonic resonance for crack imaging.

Previous experimental studies considered higher harmonics or subharmonics individually for the analysis of cracked interface. Either one of them were frequently ignored. The reason for not being able to extract both harmonic components together in one measurement can be attributed to bandwidth limit of receiving transducers. The present study is concerned with simultaneous measurements of nonlinear harmonic components at cracked interfaces in absolute manner. For this purpose, we fabricated broadband Lithium Niobate ($LiNbO_3$) transducers. We also developed a calibration technique for making absolute amplitude measurements with fluid-coupled receiving transducers [18].

This paper is outlined as follows. First, a calibration technique for absolute amplitude measurements is provided. Then, experimental details for extracting both subharmonic and higher harmonic components from a cracked compact tension (CT) specimen are described. Finally, we present simulation results based on the existing interface model to explain the observed nonlinear behavior.

HARMONIC GENERATION EXPERIMENT

Figure 1 is a schematic representation of the calibration measurement that is performed prior to the harmonic generation measurement. The purpose of the calibration measurement is to obtain the output signal in terms of the absolute displacement amplitude in the harmonic generation experiment. We use the concept of transfer function $H(\omega)$ that converts the electric output (current) $I_{out}(\omega)$ to the absolute displacement amplitude $A_{inc}(\omega)$ at the reception side of a contact ultrasonic measurement through the following relationship:

$$A_{inc}(\omega) = H(\omega) I_{out}(\omega) \tag{1}$$

This transfer function can be obtained during the calibration phase using a broadband pulse-echo technique. The broadband calibration pulse is produced by a commercial pulser (Panametrics 5052 PR pulser/receiver). This broadband technique establishes empirical conversion efficiency for the receiving transducer as a function of frequency, allowing the direct calculation of the displacement amplitudes. The calibration procedure consists of measuring the voltage, $V'_{in}(\omega)$, and the current, $I'_{in}(\omega)$, applied to the receiving transducer by a broadband pulser and the output voltage, $V'_{out}(\omega)$, and current, $I'_{out}(\omega)$, from the same transducer after the input pulse has made one round trip through the sample. Assuming the reciprocity of transducer/couplant arrangement and linearity of the measurement system, the transfer function is obtained as [18]

$$H(\omega) = \sqrt{\frac{\left| I'_{in}(\omega)\left(\frac{V'_{out}(\omega)}{I'_{out}(\omega)}\right) + V'_{in}(\omega) \right|}{2\omega^2 \rho v a |I'_{out}(\omega)|}} \tag{2}$$

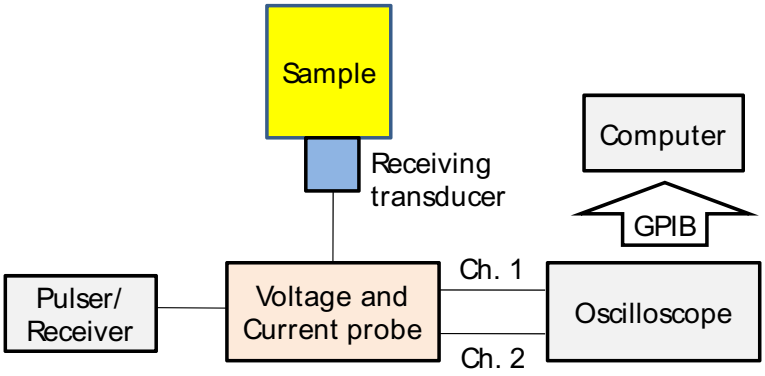

FIGURE 1. Schematic diagram for calibration of receiving transducer.

where ω is the circular frequency, ρ is the density, v is the longitudinal velocity, and a is the area of the transducer. Here the prime is used to denote a parameter measured during the calibration. Note that the transmitting transducer must not be coupled to the sample during the calibration stage, as a free surface reflection is required to maintain reciprocity. A diffraction correction is applied to the calibration measurement for $H(\omega)$ when the round trip distance through a sample is greater than the distance to the nearfield/farfield transition.

Once the calibration measurements are made, the transmitting transducer is coupled to the sample for the transmission measurement. A monochromatic toneburst at the fundamental frequency is injected into the sample, propagates along the length of the sample and is received by the receiving transducer. The absolute displacement amplitude of the transmitted wave incident on the receiving transducer is calculated from the output current, $I_{out}(\omega)$, using Eq. (1). Figure 2 shows an equipment block diagram of the harmonic generation measurement system. A function generator (Marconi 2022D) tuned to the fundamental frequency (10 MHz for these measurements) supplies the continuous wave for a gated amplifier (Matec 5100/515A) to provide the high power monochromatic toneburst for the harmonic generation. The two transducers are made of $LiNbO_3$ wafers (longitudinal polarization) and coupled to the sample with a light oil. The size of the transducer is 12.7 mm in diameter. The transmitter has a center frequency of 10 MHz, while the receiver has a broad bandwidth with a center frequency of 15 MHz. The two transducers are aligned with each other by being placed in a test fixture that can provide a constant pressure during the entire measurement.

The harmonic generation measurements have been made at eight different input fundamental amplitude by using a stepped attenuator (0, 1, 2, 3, 4, 5, 6, 10 dB) in the circuit between the gated amplifier output and the transmitting transducer. The nonlinearity parameter for the first subharmonic component ($\beta'_{1/2} = A_{1/2}/A_1^2$) is obtained from the slope of the $A_{1/2}$ versus A_1^2 plot. Similarly, the nonlinearity parameter for the second harmonic component ($\beta'_2 = A_2/A_1^2$) is obtained from the slope of the A_2 versus A_1^2 plot. Here, A_1 , $A_{1/2}$ and A_2 represent the magnitude of Fourier spectrum of the received wave at the fundamental (f=10 MHz), the first subharmonic (f/2=5 MHz), and the second harmonic frequency (2f=20 MHz), respectively.

A compact tension (CT) specimen of Al 6061-T6 is used in this work. This cracked specimen was fabricated by applying a high cycle fatigue loading on a chevron notch. Figure 3 shows the schematic configuration of the cracked CT specimen. The crack length was measured to be about 40 mm from the notch center.

Harmonic generation measurements are made in the through transmission mode at six different positions along the cracked interface as shown in Fig. 4. The measurement interval in this case is 5 mm.

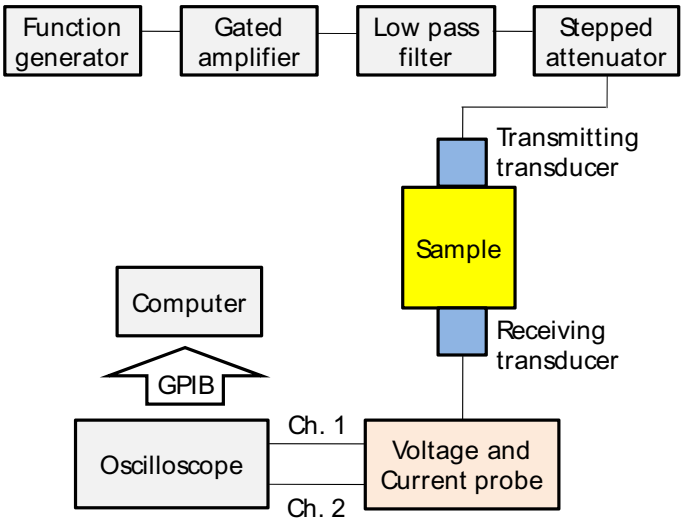

FIGURE 2. Schematic diagram for harmonic generation measurement.

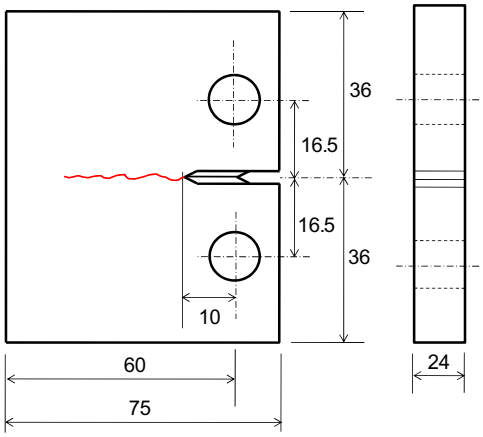

FIGURE 3. Configuration of CT specimen with fatigue crack (unit: mm).

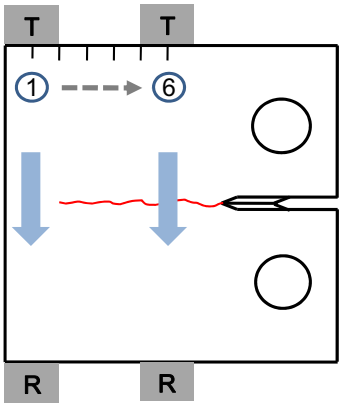

FIGURE 4. Harmonic generation measurements at six positions along the cracked interface.

RESULTS AND DISCUSSION

Figure 5 shows a typical transfer function obtained with the calibration measurement system. This function is acquired from the measurement at the position 1 on the cracked CT specimen (Fig. 4) and used for the calibration purpose in harmonic generation measurements at all six positions. It is noted that the receiving transducer seems to have a broad bandwidth in the region of interest (5-25 MHz).

The received signals before and after calibration are shown in Fig. 6 together with corresponding Fourier spectra. This signal is obtained from the measurement position 2. The input signal used is the monochromatic toneburst of the center frequency f=10 MHz, and amplified with a gated amplifier up to 150 $V_{p\text{-}p}$. This value corresponds to the 0 dB amplification out of eight different input levels used. The received signal is then calibrated using the transfer function. After calibration, the absolute displacement of the output signal turned out to be about 60 nm peak-to-peak as shown in Fig. 6(b). In addition to the fundamental component at f=10 MHz, both the first subharmonic and the second harmonic components are clearly seen at $f/2$=5 MHz and $2f$=20 MHz. Thus, the amplification voltage of 150 $V_{p\text{-}p}$ seems to be above the harmonic generation threshold. It can be also noticed that the subharmonic intensity becomes almost the same as the second harmonic intensity after calibration of the received signal. We focus on these two harmonic components in further discussion below for nonlinearity parameter variation along the crack surface.

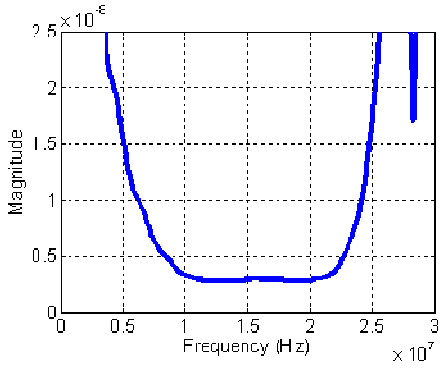

FIGURE 5. Example of a typical transfer function.

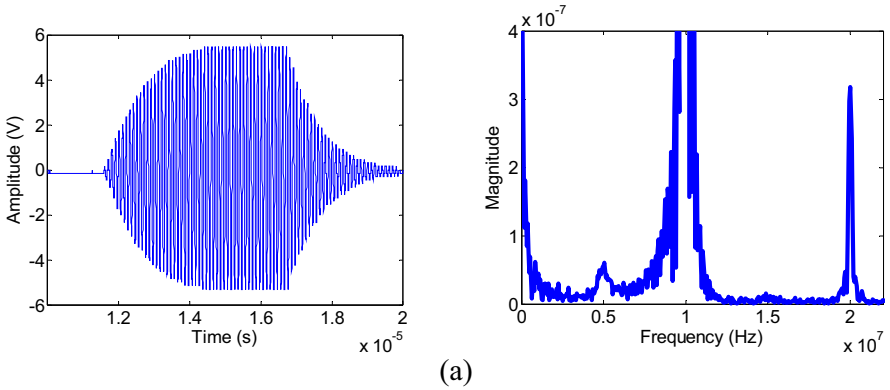

(a)

FIGURE 6. Harmonic generation measurement at position 2 with 0 dB input excitation: (a) Received waveform and Fourier spectrum before calibration.

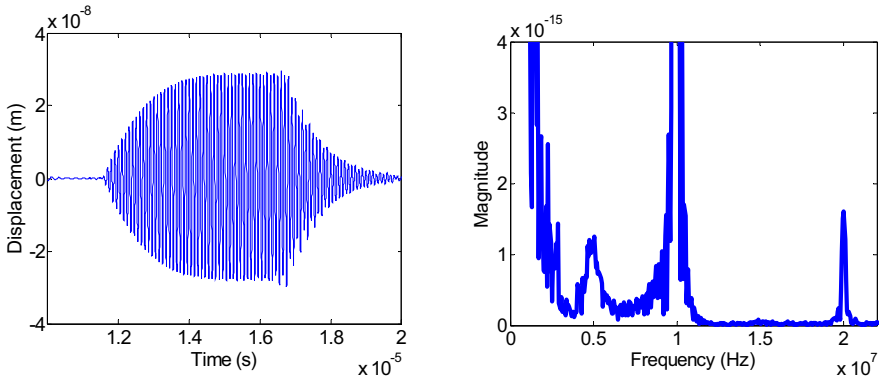

(b)

FIGURE 6. Harmonic generation measurement at position 2 with 0 dB input excitation: (b) Received waveform and Fourier spectrum after calibration.

The measured nonlinearity parameter for the subharmonic component ($\beta'_{1/2}$) and for the second harmonic component (β'_2) are shown in Fig. 7 before and after calibration. Both parameters are seen to be very small near the crack end and then increase rapidly as the measuring point moves toward the crack opening direction. The results of the second harmonic nonlinearity (β'_2) are qualitatively consistent with the previous work by Lee and Jhang [11] where, using the uncalibrated receiving transducer output signal, the ratio of the second harmonic to the square of the fundamental also decreased toward the crack end. This behavior can be expected because a certain part of the crack produced by the fatigue loading can be treated as a partially closed crack and they will act as interface harmonic generators of different level. If the crack is too open to transmit the incident wave, most of the incoming wave will be reflected from the crack surface. The degree of harmonic generation will depend on the roughness of the surface and on the magnitude of the cohesive forces that arise from the small crack openings. This dependence will be further discussed in the model simulation below.

When the calibrated received signal was used in the nonlinearity parameter calculation, the subharmonic components provide higher nonlinearity parameters than those of the second harmonic components (Fig. 7(b)). Therefore, subharmonic response could be used as more reliable indicators in detecting crack-like flaws.

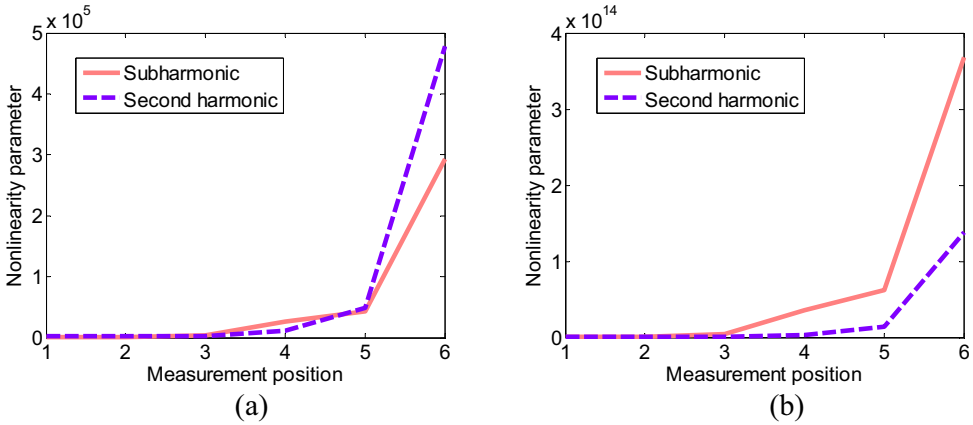

(a) (b)

FIGURE 7. Variation of nonlinearity parameter as a function of measurement position: (a) Before calibration, (b) After calibration.

MODEL PREDICTION FOR HARMONIC GENERATION

Sasaki et al. [19] proposed a nonlinear dynamic model for a partially closed crack when the wavelength is much longer than the crack size. They assumed that harmonics are generated by the clapping between the input and output crack planes. Their model was used for simulation of subharmonic generation at a surface-breaking crack under bending loads. In the model, the input crack plane vibrates with predetermined amplitude and frequency in the form of $a\sin\omega t$, while the output crack plane is represented by the mass m and the spring of stiffness k. When the input crack plane vibrates with a sufficiently large amplitude, this crack plane displaces the output crack plane by contact. Thus, the input crack plane exerts an interaction force on the other crack plane, depending on the crack opening displacement (COD). Under the harmonic excitation, the equation of the motion of the output crack plane is given by [19]

$$m\ddot{x} + \gamma\dot{x} + k(x - x_s) = f_0\left[\kappa\left(\frac{\sigma}{x - a\sin\omega t}\right)^M - \left(\frac{\sigma}{x - a\sin\omega t}\right)^N\right] \quad (3)$$

where $x(t)$ is the position of the output crack plane, a is the input wave amplitude, ω is the input wave frequency, γ is the viscosity of vibration and x_s is the equilibrium position of the output crack plane without the interaction force. In Eq. (3) f_0 is the magnitude of force, M is the repulsive force index, N is the attractive force index, κ is the weight of repulsive force relative to attractive force and σ is the characteristic length of crack plane (e.g., interatomic distance, grain size or asperity height, etc.).

Figure 8 shows calculated input and output waveforms and their frequency contents. Numerical values for various parameters were M=9, N=3. κ=1, f_0=30σ, ω=1, a=15σ, m=1, k=0.2, and γ=0.5. The output waveforms are plotted with x_s=11σ. In the plot of input waveform, the time scale was adjusted to have a period corresponding to the fundamental frequency of f=10 MHz. The amplitude scale was normalized by σ.

In the power spectrum of output signal (Fig. 8(b)), frequency components of the first subharmonic wave (f/2=5 MHz) and ultra-subharmonic wave (3f/2=15 MHz) are observed. Higher harmonic components of 2f=20, 3f=30 MHz are also clearly seen. The intensity of the first subharmonic wave at f/2 is found to be slightly larger than that of the second harmonic wave at 2f. Thus, except for the relatively low power spectrum (or amplitude) at fundamental frequency f, this nonlinear dynamic model for cracked interfaces seems to predict well the harmonic generation behavior observed at the real fatigue crack of CT specimen (Fig. 6).

CONCLUSIONS

Harmonic generation at a real cracked interface of a compact tension (CT) specimen was studied in this work. Two dominant harmonic components were experimentally identified as

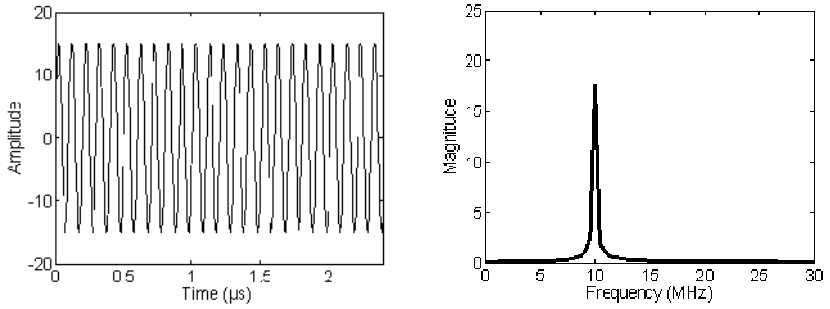

(a)

FIGURE 8. Simulation results for harmonic generation at a crack interface: (a) Input waveform and Power spectrum.

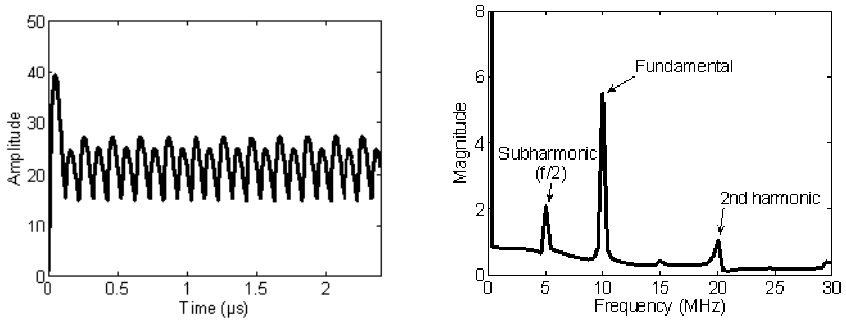

(b)

FIGURE 8. Simulation results for harmonic generation at a crack interface: (b) Output waveform and power spectrum.

the first subharmonic at frequency *f*/2 and the second harmonic at 2*f* with the interrogation signal of frequency of *f*. Nonlinear parameters of these two harmonics were defined and measured at several positions on the specimen, and showed a variation that is consistent with a gradually closing crack toward the crack end. In the present study, the nonlinearity parameter of *f*/2 generally had a higher value after calibration of output signals. This means that the subharmonic can be a good indicator for detecting closed cracks. We are going to further study the optimal generation of the subharmonics for more reliable detection and characterization of crack-like flaws.

ACKNOWLEDGEMENT

This work was supported by the Nuclear R&D program through the National Research Foundation of Korea (NRF) funded by the Ministry of Education, Science and Technology.

REFERENCES

1. K.-Y. Jhang, *Int. J. Precision Engineer. Manufactur.*, **10**, pp. 123-135 (2009).
2. J. M. Richardson, *Int. J. Engineer. Sci.*, **17**, pp. 73-85 (1979).
3. J. D. Achenbach and A. N. Norris, *J. **Nondestr**. **Eval**.*, **3, pp. 229**-239 (1982).
4. S. Hirose and J. D. Achenbach**, *J. Acoust**ic.** Soc. Am.*, **93**, pp. 142-147 (1993).
5. O. Buck, W. L. Morris and J. M. Richardson, *Appl. Phys. Let.*, **33**, pp. 371–373 (1978).
6. J. H. Cantrell and W. T. Yost, *Int. J. Fatigue*, **23**, pp. 487-490 (2001).
7. D. J. Barnard, G. E. Dace and O. Buck, *J. Nondestr. Eval.*, **16**, pp. 67-75 (1997).
8. K. Y. Jhang, *IEEE-UFFC*, **47**, pp. 540- 548 (2000).
9. H. Jeong, S. H. Nahm, K. Y. Jhang and Y. H. Nam, *Ultrasonics*, **41**, pp. 543-549 (2003).
10. W. L. Morris, O. Buck and R. V. Inman, *J. Appl. Phys.*, **50**, pp. 6737-6741 (1979)
11. T. H. Lee and K.-Y. Jhang, *NDT&E Int.*, **42**, pp. 757–764 (2009)
12. A. Wegner, A. Koka, K. Janser, U. Netzelmann, S. Hirsekorn and W. Arnold, *Ultrasonics*, **38**, pp. 316-321 (2000)
13. M. Rothenfusser, M. Mayr and J. Baumann, *Ultrasonics*, **38**, pp. 322-326 (2000)
14. P. M. Shankar, P. D. Krishna and V. L. Newhouse, ***J**. **Acoust**ic. **Soc**. **Am**.*, **106**, pp. 2104-2110 (1999).
15. A. Moussatov, V. Gusev and B. Castagne`de, *Phys. Rev. Let.*, **90**, pp. 124301-1~4 (2003).
16. F. Semperlotti, K. W. Wang and E. C. Smith, *Appl. Phys. Let.*, **95**, pp. 254101 -1~3 (2009).
17. K. Yamanaka, T. Mihara and T. Tsuji, *Jap. J. Appl. Phys.*, **43**, pp. 3082-3087 (2004).
18. G. E. Dace, R. B. Thompson and O. Buck, *Review of Progress in QNDE,* **11**, pp. 2069-2076 (1992).
19. R. Sasaki, T. Ogata, Y. Ohara, T. Mihara and K. Yamanaka, *Jap. J. Appl. Phys.*, **44**, pp. 4389-4393 (2005).